Joint EUROGRAPHICS - IEEE TCVG Symposium on Visualization (2002)
D. Ebert, P. Brunet, I. Navazo (Editors)

Direct Volume Rendering of Photographic Volumes Using Multi-Dimensional Color-Based Transfer Functions

Christopher J. Morris David Ebert

IBM TJ Waston Research Center† Purdue University‡

Abstract

Traditionally, volume rendering of medical data has been comprised of transfer functions that map a scalar value, usually a MRI or CT intensity, to an opacity. Corresponding color maps are either selected regardless of the actual physical color of the volume (i.e. greyscale) or predetermined as in photographic volumes. Rarely has the voxel color been used as a means to define the associated opacity value. By using transfer functions that map multi-channel color values(RGB or CIE $L^*u^*v^*$) to opacity, we can generate compelling and informative renderings that provide consistent boundary extraction throughout the volume. We present renderings of the Visible Human photographic volume using multi-dimensional color-based transfer functions. These functions were constructed by using gradient boundary enhancement techniques in conjunction with volume illustration techniques and incorporating the first and second directional derivatives along the gradient direction. We empirically compare the effectiveness of using the color-based transfer functions and discuss their applications and potential for future development.

Categories and Subject Descriptors (according to ACM CCS): I.3.5 [Computer Graphics]: Boundary Representation I.3.7 [Computer Graphics]: Raytracing I.3.8 [Computer Graphics]: Applications

1. Introduction

Increasingly, photographic volumes are becoming a viable and important means to represent anatomical and pathological information. Not only is the ability to acquire and compose data in this manner progressing but, the advantages that they hold over traditional data acquisition techniques(i.e. CT, MRI) have been further realized. A lack of adequate resolution provided the impetus for the Whole Frog Project at Lawrence Berkeley National Laboratory to use photographs of cryosections to create a volume dataset of an entire frog[26]. Other examples of cryosection imaging can be found at UCLA's Laboratory for Neurological Imaging and the Armed Forces Institute of Pathology's Visible Embryo Project. The most comprehensive examples of data acquisition using photographic tomographic imaging are the Visible Female and Visible Male datasets produced by the National Library of Medicine[36].

The Visible Human datasets were created as part of a project to study the potential of using photographic volumes in anatomy research and education. Computed tomography(CT), magnetic resonance imaging (MRI), and plain film radiographs were used to collect data from both a male and female subject. The subjects were then frozen and sectioned in 1 mm and 1/3 mm axial intervals for the male and female subjects, respectively. These sections were subsequently photographed with 35mm and 70mm film and digitized using an electronic camera. The resulting resolution of the digital images is 2048x1216 and 4096x2700 for the data generated from the 35mm and 70mm film, respectively. These datasets represent one of the most complete and extensive anatomical studies ever performed.

With the availability of these high-resolution datasets, an interesting problem develops of how to effectively render

† (cjmorris@us.ibm.com) Visual Technology, IBM TJ Watson Research Center,19 Skyline Drive, Hawthorne, NY 10532, USA

‡ (ebertd@purdue.edu) School of Electrical and Computer Engineering, Purdue University,1285 EE Building, West Lafayette,IN 47907, USA

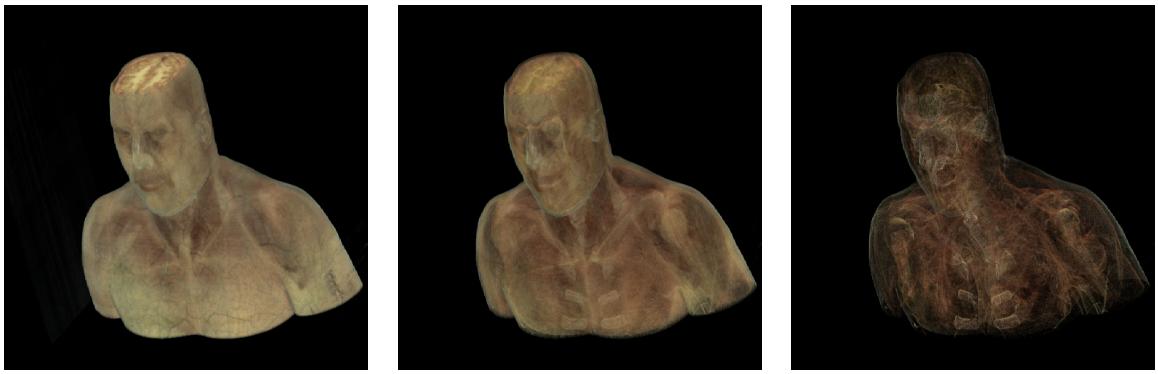

Figure 1: *Renderings of the head and upper torso from using the CIE L^* gradient magnitude function.* ***Left)*** *k_{gc}=0.25, k_{gs}=0.5, k_{ge}=1.0.* ***Center)*** *k_{gc}=0.0, k_{gs}=0.75, k_{ge}=1.0.* ***Right)*** *k_{gc}=0.0, k_{gs}=0.75, k_{ge}=1.5* ***<see color section>****.*

these volumes in a fashion that yields information previously not obtainable from "traditional" clinical data sets or volume rendering methods. Recently, color-based transfer functions were designed that would facilitate the generation of compelling volume renderings of these datasets. These transfer functions were based solely on the three channel color space (RGB or CIE $L^*u^*v^*$) of the photographic datasets. Both color distance gradient magnitudes and color distance gradient dot products were used to map the voxel's color information to an opacity value. When coupled with volume illustration techniques[5], where a physics-based illumination model is used in conjunction with non-photorealistic rendering (NPR) methods, there is the potential for a powerful technique in which to convey the structure of a photographic volume model.

Though these transfer functions succeed in extracting many boundaries within the volume, the opacity of a voxel was largely based on the gradient magnitude at that voxel. For a more exact determination of a boundary region, another measure is needed. It has been demonstrated that volumes of scalar data suggest their own appropriate transfer function when boundaries between different materials are the primary regions of interest[17]. Furthermore, these transfer functions can be determined by the relationship between the original data value and the first and second directional derivatives along the gradient direction. This notion applies to photographic volumes where the data values are the color components and a significant change in these color components denotes a boundary of some sort. We build upon the utility of the color-based transfer functions and the volume illustration techniques by applying them simultaneously and adding a component based on the second directional derivative, namely the zero-crossing within this derivative. By adding this component, we have strengthened our method for determining boundaries within a photographic volume and subsequently, our renderings from photographic volumes. We demonstrate these advancements using the Visible Male dataset and apply these techniques to the CIE $L^*u^*v^*$ colorspace (Figure 1).

2. Related Work

2.1. Volume Rendering from Photographic Volumes

Based on previous transfer function research[4, 22, 2], techniques for creating transfer functions from the color components present in a photographic volume have been recently developed[3]. In this work, informative volume renderings were generated from photographic volumes without the need of any supplementary information from CT or MRI data as is commonly the case with volume rendering of medical data[10, 37, 39, 29, 38, 42]. Transfer functions based on the color distance gradient magnitude and the dot product of the color distance gradient and that of a neighboring voxel were effective in capturing muscle detail, bone, fat, and other tissue. This work was significant in that it offered a new approach to investigating color volume data. Previous rendering techniques that used the Visible Human color photograph volume involved extracting isosurfaces from a scalar color value[23] using the Marching Cubes algorithm[24], applying a solid texture of the color volume to extracted polygons[12], and rendering based on hand-segmented volume color data[43]. In these instances, surfaces were being rendered as opposed to volumes. Volume rendering of the RGB color volume has been performed by assigning opacity values that were based on the voxel's original color intensity value[15]. This approach did not take into account the changes in intensity within the volume (i.e. the gradients) thus, boundaries between voxels of contrasting colors were not extracted.

When searching for boundaries between contrasting colors, the choice of which colorspace to search is an important one. The CIE $L^*u^*v^*$ colorspace is more accurate in capturing anatomical structures within the Visible Male photo-

graphic dataset. This greater level of accuracy, in comparison to the RGB colorspace, is due to CIE $L^*u^*v^*$'s correspondence to the human visual system and its perceptually uniform representation of the photographic color volume. A perceptually uniform colorspace is important when rendering photographic volumes because it facilitates the creation of opacity transfer functions that emphasize features that are detectable by the human visual system. Therefore, the resulting volume rendering reveals features and structures that correspond to how human vision would perceive them. In contrast, the RGB colorspace (a device-derived colorspace) will tend to falsely emphasize changes in regions of high brightness or high blue content.

2.2. Volume Illustration

In order to enhance the structural perception of volume models, a framework[5] was developed that augmented physics-based rendering methods[16, 2, 21] with NPR techniques[41, 34]. The use of this framework can generate various illustration styles using local and global properties of the volume that can enhance the perception of structure, shape, depth, and orientation within the model. Traditional volume rendering methods[2] made use of transfer functions that were not physics based and generated artificial views of data to feature particular areas of interest. Designing such transfer functions is often problematic due to the necessity of *a priori* knowledge of the model and its internal structure.

Many[16, 28, 6, 20, 40, 25, 27] have sought to develop volume rendering techniques based on realistic phenomena such as physics-based illumination and atmospheric attenuation models. NPR techniques have been extensively used to illustrate surface shape and display data. Specifically, the identification and rendering of silhouettes and boundaries has been investigated by numerous researchers[32, 34, 8, 14] and expressive textures have been applied to surfaces to denote surface shape[31, 33, 13]. However, with a few exceptions[32, 14, 13, 5], these NPR techniques and studies have been limited to the rendering of surfaces. We seek to make use of these illustration techniques to render photographic volumes. Of particular importance to the work presented in this paper, is the ability to enhance features such as boundaries and surface orientations.

2.3. Multi-Dimensional Transfer Functions

Since the existence of volume rendering, developing processes to generate informative renderings of the underlying structures within the volume model has remained an active area of research. Transfer functions are a way to systematically assign a renderable quantity (i.e. color, opacity, brightness) to a region based on the original data value of that region. It is intended that these assignments will lead to an effective rendering of the internal structures of the volume model. Designing transfer functions that are pertinent to a particular volume model is not an easy task. Several researchers[7, 11, 17] have extensively investigated methods in which to develop transfer functions that are effective in rendering volume data without prior knowledge of the data.

A transfer function that will successfully extract and render boundaries can be created from the relationship between the data value at a specific region of interest (i.e. voxel) and its first and second directional derivatives along the gradient direction[17]. Recently, these multi-dimensional transfer functions were implemented to achieve informative volume renderings in an interactive system[19]. Previously developed color-based transfer functions[3] did not incorporate the second directional derivative. Doing so can further enhance the algorithms' abilities to highlight boundaries within the color volume model, leading to an increase in the information obtained.

3. Transfer Function Construction

As mentioned previously, constructing effective transfer functions is a difficult problem. To effectively create images from photographic volumes, we have implemented techniques for boundary and oriented feature enhancement, as well as, directional derivative based techniques.

3.1. Boundary Feature Enhancement Using Color Distance Gradients

Boundary feature enhancement has been used in scientific illustration and art for centuries. These techniques are also widely used in computer graphics. The techniques of boundary enhancement and gradient-based shading were first introduced to visualization in 1988[2, 22]. We use an adaptation of these methods and allow the user to selectively enhance the density of each volume sample by a function of the gradient. We define the boundary-enhanced opacity for the voxel with the following equation:

$$opacity = o_v(k_{gc} + k_{gs} * (\|\nabla \vec{V}o\|)^{k_{ge}}) \quad (1)$$

where o_v is the original intensity values (i.e. a scalar color component) and $\|\nabla \vec{V}o\|$ is the gradient magnitude. This equation allows the user to select a range of effects from no gradient enhancement ($k_{gc} = 1, k_{gs} = 0$) to full gradient enhancement ($k_{gs} >= 1$) to only showing areas with large gradients ($k_{gc} = 0$), as in traditional volume rendering. The use of the power function with exponent k_{ge} allows the user to adjust the slope of the opacity curve to best highlight the dataset.

We have found color distance gradients to be very useful for effectively conveying information from photographic volumes. We use the color distance gradient model to calculate the gradients of the photographic data. This model is similar to the color difference models described and developed independently[1, 35]. For color photographic volume data represented in CIE $L^*u^*v^*$ space, every voxel location

is mapped to a color, represented by three separate values. As we mentioned before, CIE $L^*u^*v^*$ space has reparameterized color space so that for unsaturated colors, the perceptual distances between two colors is, to a good approximation, proportional to the length of the straight line joining them. In other words, the color space is approximately locally linear. It should be noted that the difference of two adjacent colors is itself a color vector, or can be considered to be a location in the perceptually linear color space. We can then determine the distance between two colors using the general Euclidian distance formula. This converts the vector color field into a scalar field. Given this scalar field, we can use central differences as an approximation of the gradient of the field.

3.2. Color Distance Gradient Dot Products

The color distance gradient magnitude only captures changes in the length of the color distance gradient vector, not changes in its spatial orientation. We can look at the changes in the gradient of the color distance field as another feature indicator. The angular separation between the color difference gradients of two neighboring voxels is inversely proportional to the dot product of their normalized color difference gradient vectors. Therefore, to highlight areas of large angular variation of color difference gradient vectors, the following transfer function can be used:

$$opacity = \max_{i=1}^{6}[(1 - \nabla\vec{Vo} \cdot \nabla\vec{Vi}) * \|\nabla\vec{Vo}\|] \qquad (2)$$

where $\nabla\vec{Vo}$ and $\nabla\vec{Vi}$ are the normalized color distance gradient vectors of the current and neighboring voxels, respectively.

Additionally, we utilize a technique that attempts to highlight small details in the data. The formula enhances areas where a combination of large magnitudes and small angular variation of the color distance gradients exists. Therefore, it highlights oriented patterns within the color data. The resulting transfer function is the following:

$$opacity = \max_{i=1}^{6}[(\nabla\vec{Vo} \cdot \nabla\vec{Vi}) * \|\nabla\vec{Vo}\|] \qquad (3)$$

3.3. Directional Derivatives Along the Gradient Direction

Another very useful feature detection method is the use of the first and second gradient directional derivatives[17]. Both the maximum of the first derivative of a scalar field in the direction of the gradient and the zero crossings of the second derivative of a scalar field in the direction of the gradient are very good boundary and feature indicators. The first derivative of a scalar field f in the gradient direction $\widehat{\nabla f}$ is, in fact, the gradient magnitude $\|\nabla f\|$:

$$\mathbf{D}_{\widehat{\nabla f}} f = \nabla f \cdot \widehat{\nabla f} = \nabla f \cdot \frac{\nabla f}{\|\nabla f\|} = \|\nabla f\| \qquad (4)$$

For the second directional derivative along the gradient direction, the gradient of the gradient magnitude is an adequate approximation. The resulting equation is:

$$\mathbf{D}^2_{\widehat{\nabla f}} f = \mathbf{D}_{\widehat{\nabla f}} f(\|\nabla f\|) = \nabla(\|\nabla f\|) \cdot \widehat{\nabla f} = \frac{1}{\|\nabla f\|} \nabla(\|\nabla f\|) \cdot \nabla f \qquad (5)$$

3.4. Transfer Functions for Photographic Volumes

The aforementioned transfer function components provide a substantial framework for effectively volume rendering photographic volumes. To demonstrate this, we construct several separate opacity transfer functions. The first function uses the gradient magnitude of the CIE $L^*u^*v^*$ color distance gradient, at each voxel, to extract boundaries by inserting this value into the boundary enhancement equation (1). In the resulting equation, o_v is the intensity value at the voxel (a CIE $L^*u^*v^*$ component) and k_{gc}, k_{gs}, and k_{ge} are user-defined variables that will either increase or decrease the opacity at boundary or non-boundary regions. Specifically, k_{ge} adjusts the slope of the opacity curve (Figure 2).

The next group of functions makes use of the first and second directional derivatives to further delineate boundaries within the volume model. A boundary exists in the region of the maximum gradient magnitude (the first directional derivative in the gradient direction). To aid in the identification of a boundary, the zero crossing of the second directional derivative in the gradient direction is used as another boundary indicator. We implement this feature indicator in the following equations:

$$opacity = o_v * (k_{gc} + k_{gs} * (1.0 - |\mathbf{D}^2_{\widehat{\nabla f}} f|)^{k_{ge}}) \qquad (6)$$

$$opacity = o_v * (k_{gc} + k_{gs} * (|\mathbf{D}^2_{\widehat{\nabla f}} f|)^{k_{ge}}) \qquad (7)$$

$$opacity = o_v * (k_{gc} + k_{gs} * (|\mathbf{D}_{\widehat{\nabla f}} f - |\mathbf{D}^2_{\widehat{\nabla f}} f|)^{k_{ge}})) \qquad (8)$$

The absolute value of the normalized second directional derivative, $|\mathbf{D}^2_{\widehat{\nabla f}} f|$, is used in these equations to distinguish areas with high rates of change from areas of small rates of change. In the first equation, (6), $|\mathbf{D}^2_{\widehat{\nabla f}} f|$ is subtracted from its maximum value. As a result, areas of relatively little change or boundaries will be rendered opaque. In equation

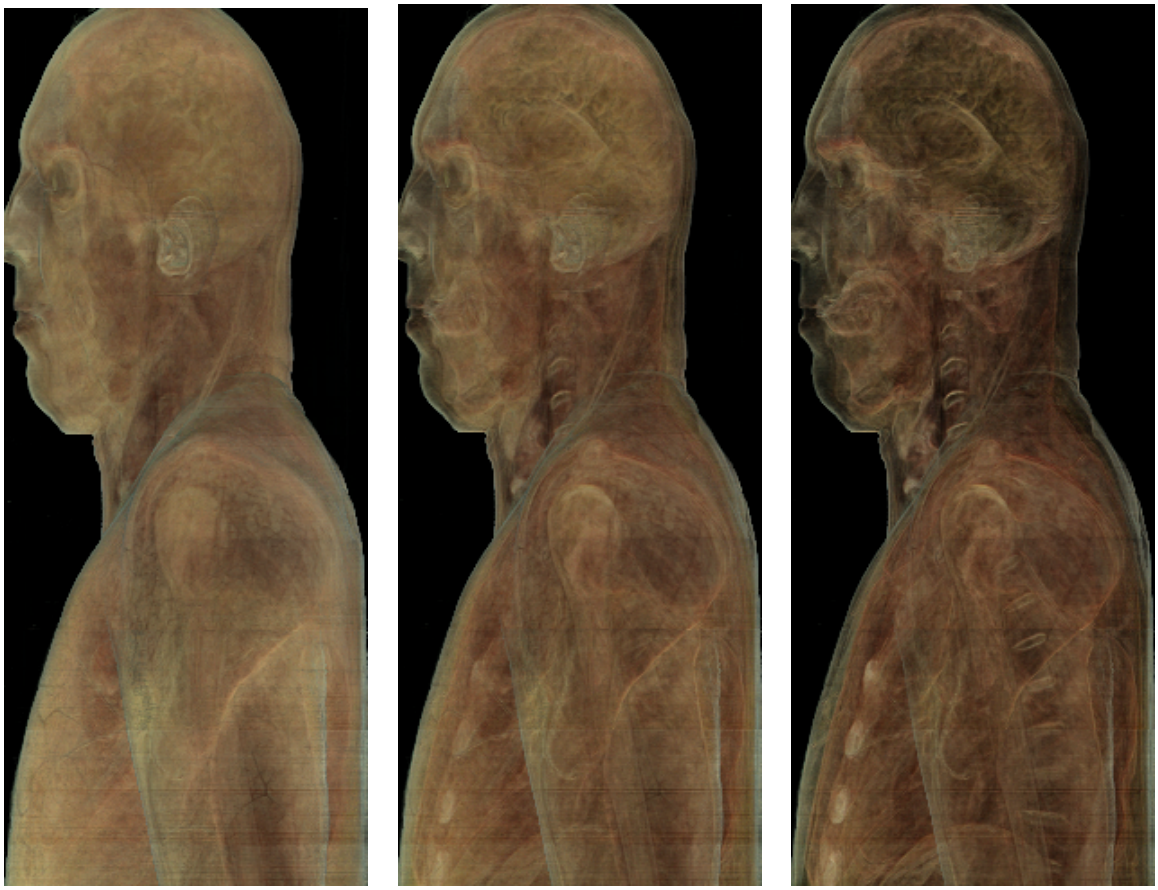

Figure 2: *Renderings of the upper torso from the side view using the gradient boundary enhancement function with k_{gc}=0.0, k_{gs}=0.75 and* ***Left)*** *k_{ge}=1.0.* ***Center)*** *k_{ge}=1.5.* ***Right)*** *k_{ge}=2.0 <**see color section**>.*

(7), only $|\mathbf{D}^2_{\widehat{\nabla f}} f|$ is used as a base for the exponential component. This will emphasize areas of high rates of change but, render zero-crossings and areas with smaller rates of change transparent. The final equation, (8), subtracts the absolute value of the second directional derivative from the first directional derivative. With this function, only areas where the gradient magnitude is the largest and the second directional derivative approximates zero will be rendered opaque, revealing the boundaries. The results of these transfer functions can be seen in Figure 3. When using equation (6), the skin becomes the most distinctive boundary and its high opacity does not allow the underlying structure to become visible. Equation (7) renders the skin transparent and some of the underlying tissue (regions close to boundaries) can be seen. However, regions, such as the skeletal structure and blood vessels, are not as evident. By implementing equation (8), much more of the underlying boundaries and structures are visible.

Finally, we developed transfer functions that implemented the color distance gradient dot product equations (2) and (3). Once again, we insert these equations into the boundary enhancement equation:

$$opacity = o_v * (k_{gc} + k_{gs} * (\max_{i=1}^{6}[1.0 - (\nabla\vec{Vo} \cdot \nabla\vec{Vi}) * \|\nabla\vec{Vo}\|]^{k_{ge}}) \tag{9}$$

In order to emphasize regions where the change in the color space is minimal (i.e. skin, muscular tissue, bone), instead of emphasizing areas where the vectors in question are nonuniform, we search for areas where the adjacent vectors are of uniform direction:

$$opacity = o_v * (k_{gc} + k_{gs} * (\max_{i=1}^{6}[(\nabla\vec{Vo} \cdot \nabla\vec{Vi}) * \|\nabla\vec{Vo}\|]^{k_{ge}}) \tag{10}$$

Using this equation, voxels that have neighboring voxels

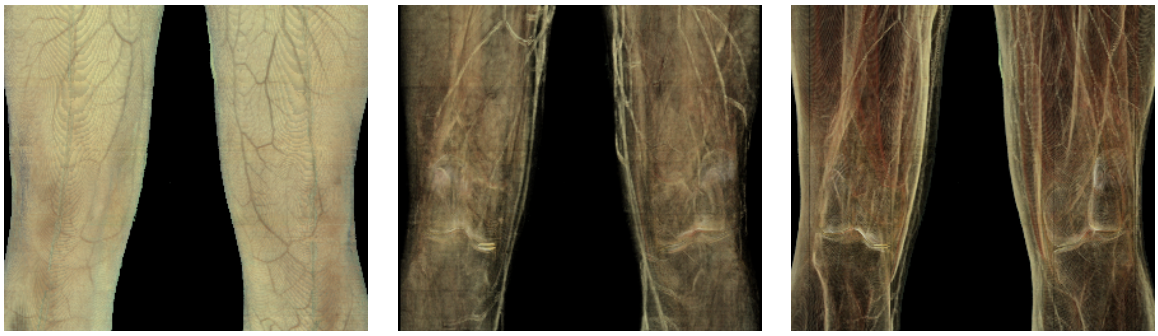

Figure 3: *Renderings of the thigh and knee regions using the transfer functions implementing the second directional derivative along the gradient.* ***Left)*** *Using equation (6).* ***Center)*** *Using equation (7)* ***Right)*** *Using equation (8). The user-defined parameters are the same in each instance,* k_{gc}*=0.0,* k_{gs}*=0.75,and* k_{ge}*=1.5* ***<see color section>****.*

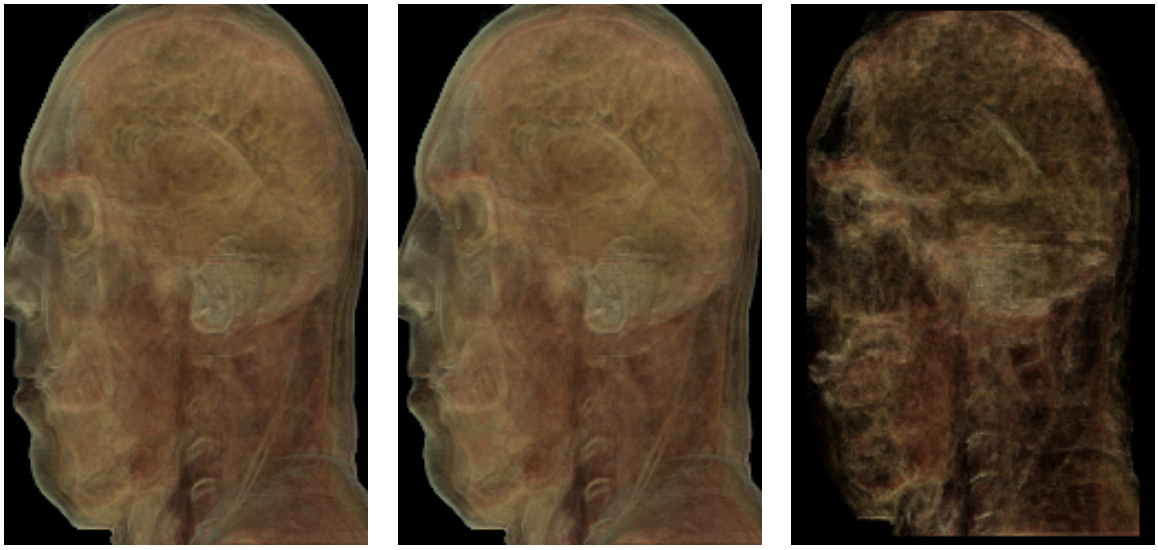

Figure 4: *Renderings of the head, from the side view.* ***Left)*** *Using equation (1),* k_{gc}*=0.0,* k_{gs}*=0.75,* k_{ge}*=1.5* ***Center)*** *Using equation (10),* k_{gc}*=0.0,* k_{gs}*=0.75,* k_{ge}*=1.5.* ***Right)*** *Using equation (9),* k_{gc}*=0.0,* k_{gs}*=1.00,* k_{ge}*=1.5* ***<see color section>****.*

with a similar color will be rendered more opaque. The results in Figure 4 reveal that equation (10) renders images that are nearly indistinguishable from images generated from the color distance gradient magnitude function (1) suggesting that areas of high gradient magnitude are also areas of relatively uniform gradient direction. Equation (9) rendered the skin and outer tissue transparent revealing more of the inner tissue (i.e. muscle, brain).

4. Applying the Transfer Functions to the Visible Male Photographic Volume

We implement the transfer functions in a ray-tracing volume renderer. The photographic volume is a subsampled volume of the original Visible Male dataset. The dimensions of our dataset are 512 x 256 pixels in the X-Y plane and 1871 slices in the Z direction. The dataset is scaled to one fourth of the original resolution to expedite the rendering process yet still retain adequate image quality. However, the rendering algorithm could easily be run using the original size dataset with the same results. The cross-sectional images in our dataset have been registered along the Z-axis using a Fast Fourier

Transform preprocessing step[30] due to the image misalignment within the original dataset. Several images that were damaged in the original volume model were excluded from our volume model. Finally, the change in brightness level between successive images, inherent in the first dataset, have not been corrected in our model and are the reason for our brightness artifacts.

The volume was constructed from Portable Pix Map(PPM) images with an 8-bit value for each of R, G, and B components at each pixel. Though we can perform our rendering algorithm on these RGB components, the CIE $L^*u^*v^*$ space is more consistent with the human visual system. As a result, the renderings presented in this paper were generated from the CIE $L^*u^*v^*$ space of the volume. The CIE $L^*u^*v^*$ components are calculated from the RGB space, in a preprocessing step[9]. We present renderings done with four of the more distinctive transfer functions (1, 7, 8, 9) at the same parameter (k_{gc}, k_{gs}, k_{ge}) values to compare and contrast their effectiveness (Figure 5). It should be noted that the final renderings will differ depending on the color component (i.e. CIE L^*, u^*, or v^*) that is used as the original intensity value, o_v, within the transfer functions. These differences, as well as the use of color-based transfer functions in the RGB colorspace, have already been investigated and discussed previously[3].

5. Discussion

It can be seen in the final renderings that basing the opacity functions on the CIE $L^*u^*v^*$ color space effectively reveals structures within the volume. Figure 2 shows three separate renderings of a side view of the upper torso of the Visible Male. In each of the renderings it is evident that the skin tissue has been made transparent as well as the muscle, fat, and bone tissues to some degree. It is clear that using the L^* component as the original intensity value, o_v, retains a significant amount of the tissue boundaries. As the exponent parameter, k_{ge}, is increased, the boundaries become more apparent.

When the opacity transfer function is varied and the color component variable and user-defined parameters remain constant, as in Figure 5, the properties of these transfer functions are revealed. The gradient magnitude transfer function (1) depicts a relatively gradual increase in the transparency of the underlying structures. Though the boundaries become more apparent as k_{ge} is increased, enough of the areas of minimal gradient magnitude are still discernible. As a result, structures can be analyzed in relation to one another.

Transfer functions (7) and (8) follow a much steeper path of increasing transparency. In the same k_{ge} intervals, the areas of minimal gradient are "quickly" rendered transparent when using equation (8). What remains are many of the boundaries of the internal structure. When using equation (7), the outer boundaries are the regions that become increasingly transparent, leaving the tissue within these boundaries visible. The color distance gradient dot product transfer function (9) has an even greater rate of transparency than transfer function (7). Though internal tissue regions are rendered, as with (7), separate regions are not as clearly delineated.

This comparative analysis illustrates the fact that effective volume renderings are dependent on the relationship between the transfer functions and the volume model itself. Obviously, a particular transfer function will not be optimal for every volume model. The opacity transfer functions discussed in this paper, will render different features within photographic volumes in different manners. The selection of which transfer function to use is also dependent on which structure the viewer wants to visualize. Furthermore, it is not readily apparent how to distinguish between regions of different tissue but similar color. Research has begun in segmenting specific tissue regions from the color volume data[18] and we plan to continue to pursue effective means to perform such operations. These transfer functions provide a foundation from which one can design optimal transfer functions for any photographic volume.

6. Conclusion

We have presented a novel approach to performing effective and informative volume rendering of color photographic volumes. This approach provides a level of detail and visual information previously unavailable with other methods. We have developed transfer functions based on the principles of volume illustration, gradient boundary enhancements, and second directional derivatives in order to extract features from the CIE $L^*u^*v^*$ color space. The resulting volume renderings of the Visible Male photographic dataset reveal internal structures and features in addition to semi-transparent external regions that allows the viewer greater insight into their relation to the overall volume.

7. Future Work

We have discussed several separate transfer functions, from how they were constructed to their effectiveness on the Visible Male dataset. These functions demonstrate the potential of volume rendering for photographic volumes. We intend to continue to investigate a number of various transfer functions that can be constructed for a host of different applications. It is also our goal to develop ways to semi-automatically design these transfer functions, as well as, develop methods to perform semi-automatic segmentation of these volumes. Furthermore, we intend to apply these transfer functions to other existing photographic volumes and to those volumes that will become available in the near future.

8. Acknowledgments

Our thanks to the Visual Technology group at IBM TJ Watson Research Center for access to and use of the Deep View Visualization Cluster, on which, these images were rendered.

References

1. Cumani, A. Edge Detection in Multispectral Images. *CVGIP: Graphical Models and Image Processing*, **53**, pp. 40-51, 1991. 3
2. Drebin, Robert A., L. Carpenter, and P. Hanrahan. Volume Rendering. *Computer Graphics (Proceedings of ACM SIGGRAPH'88)*,**22**(4), pp. 65-74, August 1988. 2, 3
3. Ebert, David, C. Morris, P. Rheingans, and T. Yoo. Designing Effective Transfer Functions for Volume Rendering from Photographic Volumes. To be published in *IEEE Transactions on Visualization and Computer Graphics*, 2002. 2, 3, 7
4. Ebert, David, T. McClanahan, P. Rheingans, and T. Yoo. Direct Volume Rendering from Photographic Data. *Data Visualization 2000(Vissym '00: Joint IEEE/Eurographics Symposium on Visualization*, pp. 137-147, Springer, May 2000. 2
5. Ebert, David and P. Rheingans. Volume Illustration: Non-Photorealistic Rendering of Volume Models. *Proceedings of IEEE Visualization '00*, pp. 195-202, October 2000. 2, 3
6. Ebert, David and R. Parent. Rendering and Animation of Gaseous Phenomena by Combining Fast Volume and Scanline A-buffer Techniques. *Computer Graphics(Proceedings of ACM SIGGRAPH '90)*, **24**(4), pp. 357-366. August 90. 3
7. Fang, Shiaofen, T. Biddlecome, and M. Tuceryan. Image-Based Transfer Function Design for Data Exploration in Volume Visualization. *IEEE Visualization '98*, pp. 319-326, October 1998. 3
8. Gooch, Bruce, P. Sloan, A. Gooch, P. Shirley, and R. Riesenfeld. Interactive Technical Illustration. *1999 ACM Symposium on Interactive 3D Graphics*, pp. 31-38, April 1999. 3
9. Hall, Roy. *Illumination and Color in Computer Generated Imagery*,Springer-Verlag, 1989. 7
10. Hauser, Helwig, L. Mroz, G. Bischi, and M. Gröller. Two-level volume rendering - fusing MIP and DVR. *Proceedings of IEEE Visualization '00*, pp. 211-218, October 2000. 2
11. He, Taosong, L. Hong, A. Kaufman, and H. Pfister. Generation of Transfer Fuctions with Stochastic Search Techniques. *Proceedings of IEEE Visualization '96*, pp. 227-234, 1996. 3
12. Imielinska, C. Technical Challenges of 3d Visualization of Large Color Data Sets. *Proceedings of the Second Visible Human Project Conference*. US Department of Health and Human Services, Public Health Service, National Institute of Health, October 7-8, 1998. 2
13. Interrante, Victoria, H. Fuchs, and S. Pizer. Conveying the 3D Shape of Smoothly Curving Transparent Surface via Texture. *IEEE Transactions on Visualization and Computer Graphics* **3**(2), April-June 1997. 3
14. Interrante, Victoria, H. Fuchs, and S. Pizer. Enhancing Transparent Skin Surfaces with Ridge and Valley Lines. *Proceedings of IEEE Visualization '95*, pp. 52-59, October 1995. 3
15. Johnson, Greg and J. Genetti Volume Rendering of Large Datasets on the Cray T3D. *1996 Spring Proceedings(Cray User Group)*, pp. 155-159, 1996. 2
16. Kajiya, James T and B. Von Herzen. Ray Tracing Volume Densities. *Computer Graphics(Proceedings of ACM SIGGRAPH '84)*, **18**(3), pp. 165-174, July 1984. 3
17. Kindlmann, Gordon and J. Durkin. Semi-Automatic Generation of Transfer Functions for Direct Volume Rendering. *1998 Volume Visualization Symposium*, pp. 79-86, October 1998. 2, 3, 4
18. Kniss, Joe, G. Kindlmann, and C. Hansen. Multi-Dimensional Transfer Functions for Interactive Volume Rendering. To appear in *IEEE Transactions on Visualization and Computer Graphics*, July 2002. 7
19. Kniss, Joe, G. Kindlmann, and C. Hansen. Interactive Volume Rendering Using Multi-Dimensional Transfer Functions and Direct Manipulation Widgets. *Proceedings of IEEE Visualization '01*, pp. 255-262, October 2001. 3
20. Kreuger, Wolfgang. The Application of Transport Theory to the Visualization of 3D Scalar Fields. *Computers in Physics*, pp. 397-406, July 1991. 3
21. Levoy, Marc. Efficient Raytracing of Volume Data. *ACM Transactions on Graphics*, **9**(3), pp. 245-261, 1990. 3
22. Levoy, Marc. Display of Surfaces from Volume Data. *IEEE Computer Graphics and Applications*, **8**(5), pp. 29-37, 1988. 2, 3
23. Lorenson, William E. Marching Through the Visible Man.. *Proceedings of IEEE Visualization '95*, pp. 368-373, 1995. 2
24. Lorenson, William E. Marching Cubes: A High Resolution 3D Surface Construction Algorithm. *Proceedings of ACM SIGGRAPH '87*, **21**, pp. 163-169, 1987. 2
25. Max, Nelson. Optical Models for Direct Volume Ren-

dering. *IEEE Transactions on Visualization and Computer Graphics*. **1**(2), pp. 99-108, June 1995. 3

26. Nip, W. and C. Logan. Whole Frog Technical Report. Technial Report LBL-35331, University of California, Lawrence Berkeley Laboratory, 1991. 1

27. Nishita, Tomoyuki. Light Scattering Models for the Realistic Rendering of Natural Scenes. *Eurographics Rendering Workshop 1998*, pp. 1-10, June 1998. 3

28. Nishita, Tomoyuki, Y. Miyawaki, and E. Nakamae. A Shading Model for Atmospheric Scattering Considering Luminous Intensity Distributioin of Light Sources. *Computer Graphics(Proceedings of ACM SIGGRAPH '87)*, **21**(4), pp. 303-310, July 1987. 3

29. Park, Steven, P. Shirley, Y. Livnat, C. Hansen, and P. Sloan. Interactive Ray Tracing for Isosurface Rendering. *Proceedings of IEEE Visualization '98*, pp. 233-238, October 1998. 2

30. Reddy, B.S. and B.N. Chatterji. An FFT-Based Technique for Translation, Rotation, and Scale-Invariant Image Registration. *IEEE Transactions on Image Processing*, **5**(8),1996. 7

31. Rheingans, Penny. Opacity-Modulating Triangular Textures for Irregular Surfaces. *Proceedings of IEEE Visualization '96*, pp. 219-225, October 1996. 3

32. Saito, Takafumi and T. Takahashi. Comprehensible Rendering of 3-D Shapes. *Computer Graphics(Proceedings of ACM SIGGRAPH'95)*, **24**(4), pp. 197-206, August 1990. 3

33. Salisbury, Michael P., M. Wong, J. Hughes, and D. Salesin. Orientable Textures for Image-Based Pen-and-Ink Illustration. *Proceedings of ACM SIGGRAPH '97*, pp. 401-406, August 1997. 3

34. Salisbury, Michael P., S. Anderson, R. Barzel, and D. Salesin. Interactive Pen-and-Ink Illustration. *Proceedings of ACM SIGGRAPH '94*, pp. 101-108, July 1994. 3

35. Sapiro, Guillermo. Technical Report HPL-95-113, Hewlett-Packard Labs, 1995. 3

36. Spitzer, V. M., M. Ackerman, A. Sherzinger, and D. Whitlock. The Visible Human Male: A Technical Report. *Journal of the American Medical Informatics Association*, **3**(2), pp. 118-130, 1996. 1

37. Tam, Roger, C. Healey, B. Flak, and P. Cahoon. Volume Rendering of Abdominal Aortic Aneurysms. *Proceedings of IEEE Visualization '97*, pp. 136-145,October 1997. 2

38. Tiede, Ulf, T. Schiemann, and K. Höhne. High Quality Rendering of Attributed Volume Data. *Proceedings of IEEE Visualization '98*, pp. 255-262, October 1998. 2

39. Wan, Ming, Q. Tang, A. Kaufman, Z. Liang, and M. Wax. Volume Rendering Based Interactive Navigation within the Human Colon. *Proceedings of IEEE Visualization '99*, pp. 397-400, October 1999. 2

40. Williams, Peter and N. Max. A Volume Density Optical Model. *1992 Workshop on Volume Visualization*, pp. 61-68, 1992. 3

41. Winkenbach, Georges and D. Salesin. Computer-Generated Pen-and-Ink Illustration. *Proceedings of ACM SIGGRAPH '94*, pp. 91-100, July 1994. 3

42. You, Suya, L. Hong, M. Wan, K. Junyaprasert, A. Kaufman, S.Muraki, Y. Zhou, M. Wax, and Z. Liang. Interactive Volume Rendering for Virtual Colonoscopy. *Proceedings of IEEE Visualization '97*, pp. 433-436, Novembert 1997. 2

43. Zhou, Ruixa and E. Henderson. Visualization of the Visible Human Anatomical Images. *Proceedings of the Second Visible Human Project Conference*, US Department of Health and Human Services, Public Health Service, National Institute of Health, October 1-2, 1998. 2

Figure 5: *Renderings of the upper torso region using the L* component.* ***From top to bottom: First Row)*** *Equation (1): Color distance gradient magnitude function.* ***Second Row)*** *Equation (9): Gradient dot product function.* ***Third Row)*** *Equation (7): Second directional derivative "only" function.* ***Fourth Row)*** *Equation (8). First and second directional derivative function.* ***From left to right: Left)*** k_{gc}*=0.0,* k_{gs}*=0.75,* k_{ge}*=0.5.* ***Center)*** k_{gc}*=0.0,* k_{gs}*=0.75,* k_{ge}*=1.0.* ***Right)*** k_{gc}*=0.0,* k_{gs}*=0.75,* k_{ge}*=1.5* ***<see color section>****.*

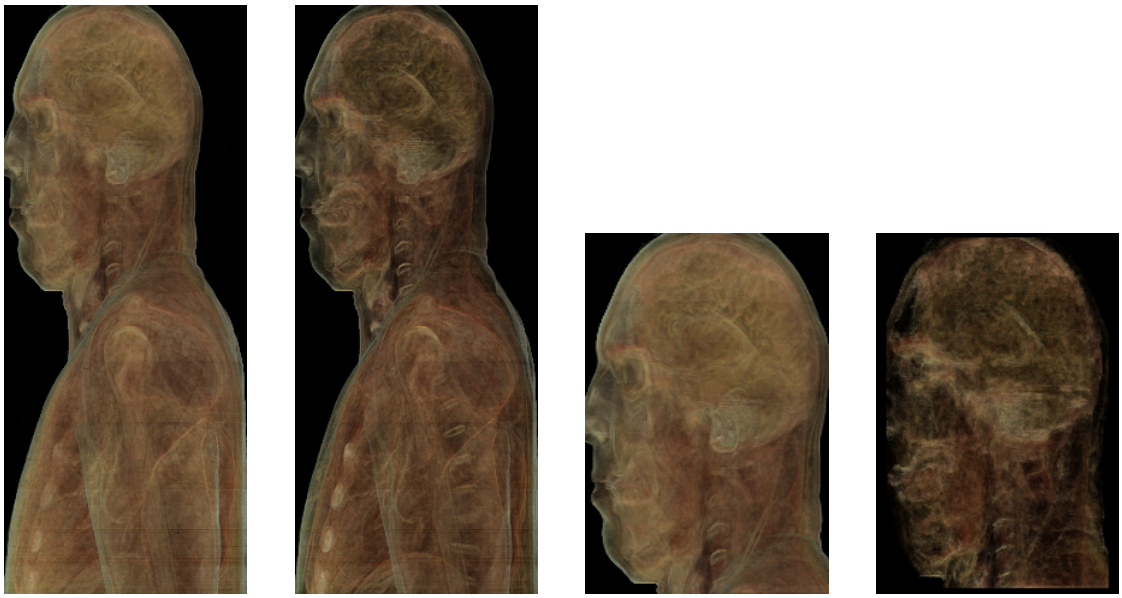

Figure 6: *Renderings of upper torso and head from side view.* ***From left to right: First)****Color distance gradient magnitude function.* k_{gc}*=0.0,* k_{gs}*=0.75,* k_{ge}*=1.0.* ***Second)*** *Color distance gradient magnitude function.* k_{gc}*=0.0,* k_{gs}*=0.75,* k_{ge}*=1.5.* ***Third)*** *Gradient dot product function for minimum angular variation.* k_{gc}*=0.0,* k_{gs}*=0.75,* k_{ge}*=1.5.* ***Fourth)*** *Gradient dot product function for maximum angular variation.* k_{gc}*=0.0,* k_{gs}*=1.0,* k_{ge}*=1.5.*

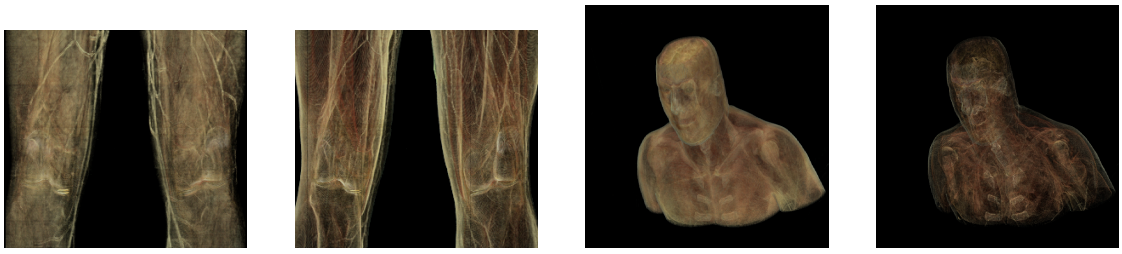

Figure 7: ***From left to right: First)*** *Renderings of the thighs and knees where* o_v *is the L* component with* k_{gc}*=0.0,* k_{gs}*=0.75, and* k_{ge}*=1.5, using the second directional derivative "only" function* ***Second)*** *Using the first and second directional derivative function.* ***Third)*** *Rendering of the upper torso where* o_v *is the L* component with* k_{gc}*=0.0,* k_{gs}*=0.75, and* k_{ge}*=1.0 and* ***Fourth)*** *Using* k_{gc}*=0.0,* k_{gs}*=0.75, and* k_{ge}*=1.5.*

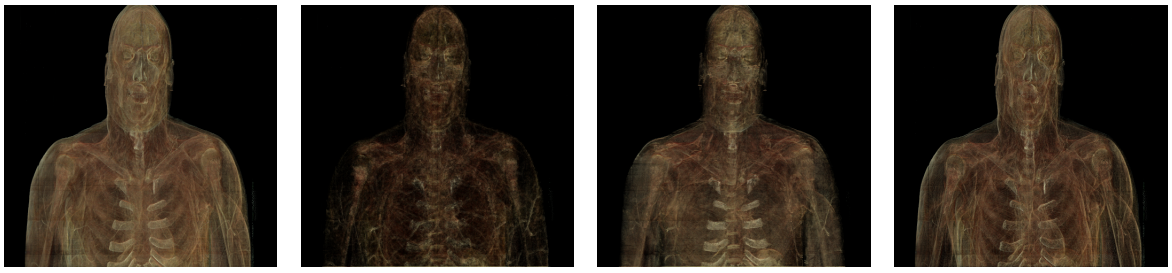

Figure 8: *Renderings of the upper torso region using the L* component with* k_{gc}*=0.0,* k_{gs}*=0.75, and* k_{ge}*=1.5.****From left to right: First)*** *Color distance gradient magnitude function.* ***Second)*** *Gradient dot product function for maximum angular variation.* ***Third)*** *Second directional derivative "only" function.* ***Fourth)*** *First and second directional derivative function.*